A Neutron Scattering Study of the Structure and Water Partitioning of Selectively Deuterated Copolymer Micelles

Cheryl M. Stancik,[†] Adrien R. Lavoie,[‡] Paulina A. Achurra,[†] Robert M. Waymouth,[‡] and Alice P. Gast*[,§]

Department of Chemical Engineering, Stanford University, Stanford, California 94305, Department of Chemistry, Stanford University, Stanford, California 94305, and Department of Chemical Engineering, Massachusetts Institute of Technology, Cambridge, Massachusetts 02139

Received December 19, 2003. In Final Form: May 2, 2004

We present a scattering study of a selectively deuterated micelle-forming diblock copolymer. The copolymer comprises a partially deuterated polystyrene (*d*,*h*-PS) block and an imidazolium-functionalized PS (IL) block. In toluene solutions, the copolymers assemble into elongated micelles where the IL block forms the micelle core. Through dynamic light scattering (DLS) measurements, we obtain the overall size of the micelles. In our small-angle neutron scattering (SANS) studies, we use contrast matching to characterize the IL core and the PS shell of the micelles independently. The PS block forming the micelle shell exhibits either a starlike or brushlike conformation depending upon the size of the core to which it is tethered. We find the IL block to be in an extended conformation, driving the formation of slightly elongated and relatively stiff micelle cores. The elongated micelle core cross-sectional radius and length depend linearly on the length of the IL block. We find that the micelles can sequester a few water molecules for each IL repeat unit; the addition of water slightly increases the cross section of the elongated micelles.

I. Introduction

The self-assembly of surfactant and copolymer molecules in solution to form micelle structures has captivated researchers for decades. A complex balance of the solvent interactions, surface tensions, and packing constraints of the assembling molecules drives this phenomenon of micelle formation.[1−3] While scientists understand the guiding principles behind micelle formation, it is the peculiarities of each system that make this a rich field of study. With the promise that micelles may be used in many applications including drug delivery,[4] catalysis,[5] and as templates for nanoparticle formation,[6] it is important that we seek out new micelle systems with novel properties that may expand or improve their utility.

Nonspherical or elongated micelles have been the subject of many detailed and interesting studies. While small molecule surfactants have been known to form nonspherical micelle geometries due to the thermodynamics of assembly, it was not until recently that block copolymers were found to form nonspherical micelle structures.[7−14] Many of these studies employed direct visualization with cryo-TEM (transmission electron microscopy) to view the elongated structures. Nonaqueous solvents make cryo-TEM challenging, complicating our ability to directly capture the true solution structure of the micelles.

While directly viewing micelle structures with microscopy is powerful, small-angle scattering techniques also allow for detailed study of elongated micelle structures. Two key advantages of scattering are that the micelle structures are observed in their solvent environment and that small length scales can be probed, often providing information regarding the structure of the individual molecules.[15,16] Both static and dynamic light scattering (SLS and DLS, respectively) have been used in detailed studies of elongated micelle structures.[17−20] Schurtenberger et al. found that the small molecule lecithin formed elongated, polymer-like micelles in organic solvents which were altered by the addition of small amounts of water.[17,18,20] A block copolymer system solvated in organic solvents was the subject of the studies by Antonietti et al. where they observed both spherical and prolate micelle morphologies depending on the copolymer composition.[19]

Small-angle neutron scattering (SANS) has proven to be particularly useful in the study of copolymer micelle systems.[21,22] The wavelengths used (typically 5−15 Å) and

* Corresponding author. E-mail: gast@mit.edu.
[†] Department of Chemical Engineering, Stanford University.
[‡] Department of Chemistry, Stanford University.
[§] Massachusetts Institute of Technology.

(1) Israelachvili, J. N. *Intermolecular and Surface Forces*; Academic Press: London, 1992.
(2) Riess, G. *Prog. Polym. Sci.* **2003**, *28*, 1107−1170.
(3) Jain, S.; Bates, F. S. *Science* **2003**, *300*, 460−464.
(4) Yang, L.; Alexandridis, P. *Curr. Opin. Colloid Interface Sci.* **2000**, *5*, 132−143.
(5) Klingelhöfer, S.; Heitz, W.; Greiner, A.; Oestreich, S.; Förster, S.; Antonietti, M. *J. Am. Chem. Soc.* **1997**, *119*, 10116−10120.
(6) Pileni, M. P. *Nat. Mater.* **2003**, *2*, 145−150.
(7) Zhang, L. F.; Eisenberg, A. *Science* **1995**, *268*, 1728−1731.
(8) Zhang, L. F.; Yu, K.; Eisenberg, A. *Science* **1996**, *272*, 1777−1779.
(9) Won, Y. Y.; Davis, H. T.; Bates, F. S. *Science* **1999**, *283*, 960−963.
(10) Chernyshov, D. M.; Bronstein, L. M.; Börner, H.; Berton, B.; Antonietti, M. *Chem. Mater.* **2000**, *12*, 114−121.
(11) Discher, D. E.; Eisenberg, A. *Science* **2002**, *297*, 967−973.
(12) Kukula, H.; Schlaad, H.; Antonietti, M.; Forster, S. *J. Am. Chem. Soc.* **2002**, *124*, 1658−1663.
(13) Zheng, Y.; Won, Y. Y.; Bates, F. S.; Davis, H. T.; Scriven, L. E.; Talmon, Y. *J. Phys. Chem. B* **1999**, *103*, 10331−10334.
(14) Won, Y. Y.; Brannan, A. K.; Davis, H. T.; Bates, F. S. *J. Phys. Chem. B* **2002**, *106*, 3354−3364.
(15) Won, Y. Y.; Davis, H. T.; Bates, F. S.; Agamalian, M.; Wignall, G. D. *J. Phys. Chem. B* **2000**, *104*, 7134−7143.
(16) Willner, L.; Poppe, A.; Allgaieri, J.; Monkenbusch, M.; Lindner, P.; Richter, D. *Europhys. Lett.* **2000**, *51*, 628−634.
(17) Schurtenberger, P.; Scartazzini, R.; Magid, L. J.; Leser, M. E.; Luisi, P. L. *J. Phys. Chem.* **1990**, *94*, 3695−3701.
(18) Schurtenberger, P.; Cavaco, C. *Langmuir* **1994**, *10*, 100−108.
(19) Antonietti, M.; Heinz, S.; Schmidt, M.; Rosenauer, C. *Macromolecules* **1994**, *27*, 3276−3281.
(20) Schurtenberger, P.; Magid, L. J.; King, S. M.; Lindner, P. *J. Phys. Chem.* **1991**, *95*, 4173−4176.
(21) Pedersen, J. S.; Svaneborg, C. *Curr. Opin. Colloid Interface Sci.* **2002**, *7*, 158−166.

10.1021/la0364183 CCC: $27.50
Published on Web 09/09/2004

Table 1. Preparation and Characterization Data for *d,h*-PS−PCMS Copolymers

	reagents				final products		
copolymer	initiator[a] (g)	xylenes (g)	monomer	monomer (g)	yield (g)	M_n[b]	PDI[b,c]
d,h-PS(125)	0.17		*d*-styrene *h*-styrene	5.40[d] 0.87[e]	4.28	13 000	1.10
d,h-PS(125)−PCMS(7)	1.00	1.70	CMS	0.72	1.01	14 100	1.17
d,h-PS(125)−PCMS(18)	1.00	1.60	CMS	1.98	0.98	15 800	1.11
d,h-PS(125)−PCMS(33)	0.60	1.60	CMS	2.38	0.77	17 700	1.14
d,h-PS(125)−PCMS(46)	0.18	1.00	CMS	1.03	0.24	19 600	1.15

[a] For *d,h*-PS(125), the initiator was the Hawker−Braslau nitroxide. For the block copolymer, the initiator was PS(125)−ONR_2, where the end group was derived from the Hawker−Braslau nitroxide. [b] As determined using GPC calibrated with linear PS standards. [c] Polydispersity index (PDI). [d] d_8-styrene. [e] h_8-styrene.

the properties of neutron contrast make SANS ideal for the study of polymeric materials, allowing the capability to employ the selective substitution of hydrogen with deuterium to highlight portions of the structures via contrast matching. Schurtenberger et al. complemented their light scattering studies described above with SANS studies to consider the details of the micelle cross section and flexibility.[17,20,23−26]

Recently, we investigated toluene solutions of a series of block copolymers comprising blocks of polystyrene (PS) and an imidazolium-functionalized PS.[27] The imidazolium-functionalized PS, that we denote as the IL block, has an imidazolium cation (3-methylimidazolium) pendant to the phenyl ring. Many imidazolium cations have the interesting property that they are ionic materials but are liquid at room temperature and often remain liquids over a wide temperature range.[28] Ionic materials with this property are classified as room temperature ionic liquids and are under intense investigation for their potential use as reactive media due to their compatibility with a diverse range of materials, low vapor pressure, and catalytic utility.[29−31] Few well-defined polymeric materials containing ionic liquid functionalities have been synthesized,[27,32,33] making our system intriguing not only for its assembly properties but also for its potential utility in applications employing ionic liquid functionalities. We anticipate that tethering an imidazolium cation to the phenyl ring of our polymeric system may alter its ionic liquid behavior; however, we believe that some of the desirable and novel properties of ionic liquid materials may be retained in these systems. Our initial study of these PS−IL block copolymers in toluene solutions with SANS and DLS indicated that they formed elongated micelle structures that had the capacity to swell with the addition of water.[27] The micelle properties determined from the SANS analysis indicated the core-forming block dictated the assembly properties of these micelles.[27]

In this work, we continue to investigate the novel behavior of the IL core-forming block more directly. We partially deuterated the PS block to assess the structure of the core and shell of the micelles independently with neutron contrast matching. Contrast matching is a powerful technique for studying copolymer micelles but has not been employed extensively, particularly in the case of nonspherical micelle structures. In this study, we present our findings on the structure and assembly properties of the cores and shells of these elongated micelles. Of particular interest is the relationship between the IL block length and the properties of the micelle cores. We complete our investigation by studying the incorporation of water into the micelles and observing its effect on the cores and shells of the elongated structures.

II. Experimental Section

II.1. Copolymer Synthesis and Characterization. The synthesis of a series of imidazolium-functionalized diblock copolymers, denoted *d,h*-PS−IL,was carried out in a three-step procedure.[27] First, a *d,h*-PS macroinitiator was prepared by the stepwise Hawker−Braslau nitroxide-mediated free-radical copolymerization of *d*-styrene and *h*-styrene to create the statistical copolymer *d,h*-PS block.[34,35] Analysis of this material by gel permeation chromatography (GPC) indicated narrow polydispersities (Table 1). This *d,h*-PS macroinitiator was then used to generate the poly(chloromethylstyrene) (PCMS) block using nitroxide-mediated living free- radical techniques to yield the *d,h*-polystyrene-*b*-poly(chloromethylstyrene) (*d,h*-PS−PCMS) diblock copolymers.[36,37] Four *d,h*-PS−PCMS copolymers were created from the *d,h*-PS macroinitiator with different PCMS block lengths. The analyses of the resultant *d,h*-PS−PCMS diblock copolymers by GPC and ^{1}H NMR allowed for the determination of the lengths of the PCMS blocks (Table 1). Finally, the reaction of these *d,h*-PS−PCMS diblock copolymers with 1-methylimidazole in *N,N*-dimethylacetamide resulted in the conversion of the PCMS block into an imidazolium-functionalized charged block with a BF_4^- counterion, which we denote as the IL block. Characterization of these *d,h*-PS−IL ionic block copolymers by ^{1}H NMR and microanalysis indicated that typically >99% of the PCMS groups were functionalized under our reaction conditions. In all cases, $NaBF_4$ was added during the functionalization step to yield the BF_4^- derivatives. The *d,h*-PS−IL ionic block copolymers were precipitated with water to afford the final products. The general synthetic procedure with the structures of the products and intermediates is shown in Scheme 1. Details of these synthetic procedures and analyses are included in the subsequent sections.

Synthetic and Characterization Methods and Materials. All synthetic manipulations were carried out using standard Schlenk techniques under an inert atmosphere. Reagent grade

(22) Castelletto, V.; Hamley, I. W. *Curr. Opin. Colloid Interface Sci.* **2002**, *7*, 167−172.
(23) Schurtenberger, P.; Jerke, G.; Cavaco, C.; Pedersen, J. S. *Langmuir* **1996**, *12*, 2433−2440.
(24) Jerke, G.; Pedersen, J. S.; Egelhaaf, S. U.; Schurtenberger, P. *Phys. Rev. E* **1997**, *56*, 5772−5788.
(25) Pedersen, J. S.; Egelhaaf, S. U.; Schurtenberger, P. *J. Phys. Chem.* **1995**, *99*, 1299−1305.
(26) Schurtenberger, P.; Magid, L. J.; Penfold, J.; Heenan, R. *Langmuir* **1990**, *6*, 1800−1803.
(27) Stancik, C. M.; Lavoie, A. R.; Schütz, J.; Achurra, P. A.; Lindner, P.; Gast, A. P.; Waymouth, R. M. *Langmuir* **2004**, *20*, 596−605.
(28) Wasserscheid, P.; Keim, W. *Angew. Chem., Int. Ed.* **2000**, *39*, 3772−3789.
(29) Rogers, R. D.; Seddon, K. R. *Ionic Liquids: Industrial Applications to Green Chemistry*; American Chemical Society: Washington, D. C., 2002; Vol. 818.
(30) Sheldon, R. *Chem. Commun.* **2001**, 2399−2407.
(31) Welton, T. *Chem. Rev.* **1999**, *99*, 2071−2083.
(32) Simmons, M. R.; Patrickios, C. S. *Macromolecules* **1998**, *31*, 9075−9077.
(33) Patrickios, C. S.; Simmons, M. R. *Colloids Surf., A* **2000**, *167*, 61−72.
(34) Hawker, C. J.; Bosman, A. W.; Harth, E. *Chem. Rev.* **2001**, *101*, 3661−3688.
(35) Benoit, D.; Chaplinski, V.; Braslau, R.; Hawker, C. J. *J. Am. Chem. Soc.* **1999**, *121*, 3904−3920.
(36) Kazmaier, P. M.; Daimon, K.; Georges, M. K.; Hamer, G. K.; Veregin, R. P. N. *Macromolecules* **1997**, *30*, 2228−2231.
(37) Lacroix-Desmazes, P.; Delair, T.; Pichot, C.; Boutevin, B. *J. Polym. Sci., Part A: Polym. Chem.* **2000**, *38*, 3845−3854.

Scheme 1. Typical Synthetic Protocol for the Generation of *ran*-*d,h*-PS Block Copolymers

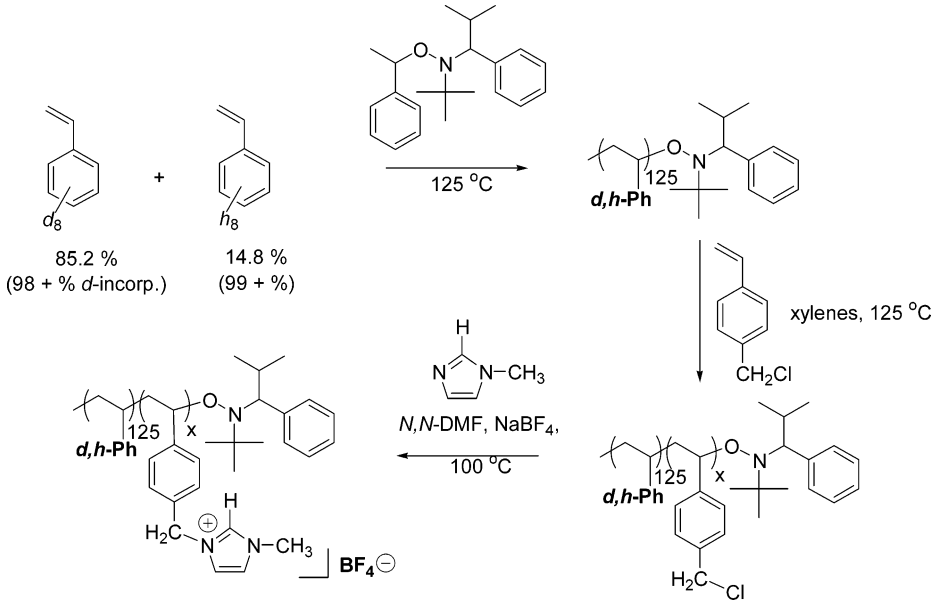

N,*N*-dimethylacetamide (Aldrich) was degassed with three freeze−pump−thaw cycles prior to use. NaBF4, 1-methylimidazole, h_8-styrene, CMS, xylenes, and toluene were obtained from Aldrich and were all used without further purification. d_8-styrene (>98%) was obtained from Acros Organics. The initiator, 2,2,5-trimethyl-3-(1-phenylethoxy)-4-phenyl-3-azahexane, was prepared according to literature procedures.[34,35]

A summary of the characterization data for the *d*,*h*-PS(125)−PCMS block copolymer precursors is given in Table 1. Deuterated DMSO (d_6, Cambridge Isotopes Laboratories, D 99.9%) and chloroform (d_1, Cambridge Isotopes Laboratories, D 99.8%) were used without further purification. ^{1}H NMR spectra were recorded on a Varian 400 MHz spectrometer, and ^{13}C{^{1}H} NMR spectra were recorded on a Varian UI300 spectrometer operating at 75.4 MHz. Chemical shifts are reported in ppm relative to residual solvent resonances (^{1}H). Gel permeation chromatography (GPC) analyses were conducted with a Millipore model 510 instrument equipped with Styragel columns. The polydispersity index (PDI) and number-average molecular weight (M_n) of the *d*,*h*-PS product were determined by the GPC analysis against linear *h*-PS standards. In our characterization of these isotopically enriched polymers, we assume that the hydrodynamic radii for h_8- and d_8-styrene are similar. Typical polymer samples were analyzed by elemental analysis (Desert Analytics, Tucson, AZ) and all values are given as percentages in the following sections.

Synthesis of *d,h*-PS. A 10 mL ampule was charged with 2,2,5-trimethyl-3-(1-phenylethoxy)-4-phenyl-3-azahexane (0.93 mol %), d_8-styrene (5.40 g, 48.15 mol), h_8-styrene (0.87 g, 8.38 mmol), and a small stir bar. The ampule was freeze−pump−thaw degassed three times and was flame-sealed under nitrogen. The ampule was then suspended in a preheated oil bath (125 °C) for 8 h followed by cooling to ambient temperature. Once cooled, the resultant material was dissolved in CH_2Cl_2 (1 mL) and was added dropwise into CH_3OH (300 mL) with vigorous stirring. The slurry was stirred for 8 h followed by isolation on a glass frit. This precipitation procedure was repeated, and the resultant white solid was evaporated under reduced pressure. The PDI and M_n of the *d*,*h*-PS product were found to be 1.10 and 13 000 g/mol, respectively. This corresponds to a degree of polymerization of 125 styrene units. To calculate the styrene degree of polymerization, we assume the isotopic composition of the *d*,*h*-PS block is equivalent to the initial styrene monomer pool ($N_{h-\text{styrene}}$ = 14.8% and $N_{d-\text{styrene}}$ = 85.2%, where N_i denotes the mole percent of component *i*). Thus, the *d*,*h*-PS(125) statistical copolymer comprises 106 *d*-PS units and 19 *h*-PS units.

Syntheses of *d,h*-PS−PCMS Copolymers. The *d*,*h*-PS(125) copolymer described above was used in these reactions. An ampule was charged with *d*,*h*-PS(125), CMS, xylenes, and a small stir bar. The relative amounts of these materials were altered to create the desired PCMS block length, as detailed in Table 1. The ampule was freeze−pump−thaw degassed three times and flame-sealed under nitrogen before suspension in a preheated oil bath (125 °C) for 0.5 h with the exception of *d*,*h*-PS(125)−PCMS(46) which was heated to 125 °C for 45 min. After cooling, the yellow material was dissolved in CH_2Cl_2 (3 mL) and was precipitated via dropwise addition to a vigorously stirred solution of CH_3OH (300 mL). The slurry was stirred for 8 h followed by isolation on a glass frit. This precipitation procedure was repeated, and the resultant white solid was evaporated under reduced pressure for at least 12 h at 50 °C. We denote the copolymer precursor products as *d*,*h*-PS(125)−PCMS(*Z*), where *Z* denotes the degree of polymerization of the PCMS block.

Typical Derivatization of *d,h*-PS−PCMS with 1-Methylimidazole. A Schlenk flask was charged with *d*,*h*-PS(125)−PCMS (700 mg), 1-methylimidazole (3.1 mL, 37.7 mmol), $NaBF_4$ (414 mg, 3.8 mmol), and dry *N*,*N*-dimethylacetamide (5.0 mL). The solution was heated at 100 °C for 7 h followed by cooling to ambient temperature. The solvent was removed at 50 °C under reduced pressure (2 days) followed by the addition of water (3 mL) with stirring for 8 h. The resultant off-white solid was isolated on a glass frit, and the precipitation and isolation procedure was repeated. We denote the products of the derivatization reactions as *d*,*h*-PS(125)−IL(*Z*), where *Z* denotes the degree of polymerization of the IL block, which we assume is not altered by the derivatization process from the PCMS degree of polymerization.

Typical NMR Characterization of *d,h*-PS−PCMS. *d*,*h*-*PS(125)−PCMS(7).* ^{1}H NMR (400 MHz, 300 K, $CDCl_3$, δ): 7.25−6.90 (11.3 H, m, Ar-*H* meta + para), 6.70−6.30 (7.2 H, m, Ar-*H* ortho), 4.51 (2.0 H, s, C*H*$_2$Cl), 2.10−1.20 (9.9 H, m, C*H*$_2$C*H*).

The relative proton integrals vary between the different copolymers according to the respective block lengths. The number of repeat units of PCMS was evaluated from the GPC data and the proton integral of the benzyl chloride protons of the PCMS block, C*H*$_2$Cl, denoted $H_{B,PCMS}$, compared to the sum of the integrals for all aromatic protons (denoted collectively as H_A) in both the PCMS and *h*-PS blocks (denoted $H_{A,PCMS}$ and $H_{A,h-PS}$, respectively). These data in combination with M_n data obtained by GPC allowed for determination of the block lengths.

We illustrate the determination of the PCMS block length for the example of *d*,*h*-PS(125)−PCMS(7). We can determine $H_{A,h-PS}$ to be 14.5 ($H_{A,h-PS} = H_A - 2H_{B,PCMS} = (11.3 + 7.2) - 2(2.0) = 14.5$) and $H_{A,PCMS}$ to be 4.0 ($H_{A,PCMS} = 2H_{B,PCMS} = 2(2.0) = 4.0$). Normalizing $H_{A,h-PS}$ and $H_{A,PCMS}$ by the number of aromatic protons per a repeat unit (i.e., five for *h*-PS and four for PCMS), we find the ratio of *h*-PS to PCMS to be 2.9:1 (*h*-PS/PCMS = (14.5/5):(4.0/4) = 2.9:1). Using the number of repeat units of *h*-PS calculated earlier (19 *h*-PS units), we can determine the PCMS block length to be about seven repeat units (i.e., 19/2.9 = ∼7). We use this procedure to calculate the block lengths of the other copolymers in the series.

d,h-PS(125)−PCMS(7). $^{13}C\{^1H\}$ NMR (75.4 MHz, 300 K, $CDCl_3$, δ): 146.5−145.0, 134.9, 129.0−127.0, 125.8, 46.3, 43.8, 41.0−40.0. We note that resonances corresponding to the various carbon nuclei were broad and were not completely differentiated in this spectrum, and as such, ranges for these resonances have been reported which correspond to various inequivalent nuclei.

Elemental Analyses of *d,h*-PS and *d,h*-PS−PCMS. *d,h-PS(125).* Anal. Calcd: C, 86.46; H(+D), 7.73; N, 0.11. Found: C, 86.02; H(+D), 7.59; N, 0.11.

d,h-PS(125)−PCMS(7). Anal. Calcd: C, 85.35; H(+D), 7.61; N, 0.11. Found: C, 85.23; H(+D), 7.20; N, 0.09.

d,h-PS(125)−PCMS(18). Anal. Calcd: C, 83.78; H(+D), 7.41; N, 0.10. Found: C, 83.56; H(+D), 7.14; N, 0.05.

d,h-PS(125)−PCMS(33). Anal. Calcd: C, 82.32; H(+D), 7.23; N, 0.09. Found: C, 81.89; H(+D), 7.25; N, 0.05.

d,h-PS(125)−PCMS(46). Anal. Calcd: C, 81.24; H(+D), 7.10; N, 0.07. Found: C, 80.16; H(+D), 6.78; N, <0.05.

Typical NMR Characterization of *d,h*-PS−IL. *d,h-PS(125)−IL(7).* ^1H NMR (400 MHz, 300 K, d_6-DMSO, δ): 9.20 (1.0 H, s, N=C*H*N), 8.10−6.20 (16.2 H, m, Ar-*H* and *H*CN=CN*H*), 5.35 (2 H, s, CH_2), 3.97 (3.0 H, s, NCH_3), 2.20−0.80 (11.5 H, m, CH_2C*H*). We note that the relative number of protons varies between the different polymers according to the respective block lengths.

d,h-PS(125)−IL(7). $^{13}C\{^1H\}$ NMR (75.4, 300 K, d_6-DMSO, δ): 146.0−145.0, 136.3, 131.8, 128.2, 124.1, 123.3, 51.7, 35.8. We note that resonances corresponding to the various carbon nuclei were broad and were not completely differentiated in this spectrum, and as before, we report ranges for these resonances which correspond to various inequivalent nuclei.

Elemental Analysis of *d,h*-PS−IL. *d,h-PS(125)−IL(7).* Anal. Calcd: C, 82.90; H(+D), 7.44; N, 1.15; Cl, 0.00. Found: C, 81.88; H(+D), 6.87; N, 1.38; Cl, <0.02.

d,h-PS(125)−IL(18). Anal. Calcd: C, 77.70; H(+D), 7.03; N, 2.75; Cl, 0.00. Found: C, 75.05; H(+D), 6.67; N, 3.08; Cl, 0.04.

d,h-PS(125)−IL(33). Anal. Calcd: C, 72.3; H(+D), 6.71; N, 4.05; Cl, 0.00. Found: C, 72.12; H(+D), 6.66; N, 4.37; Cl, <0.02.

d,h-PS(125)−IL(46). Anal. Calcd: C, 68.27; H(+D), 6.50; N, 5.40; Cl, 0.00. Found: C, 68.54; H(+D), 6.30; N, 5.58; Cl, 0.02.

These results indicate nearly quantitative conversion of the chloromethyl styrene units to imidazolium functionalities. In all cases, the counterion exchange (Cl^- to BF_4^-) was nearly quantitative (typically >99%). For the lower molecular weight samples (*d,h*-PS(125)−IL(7) and *d,h*-PS(125)−IL(18)), the measured weight percent for carbon is lower than that calculated. This is likely a consequence of the partial loss of the nitroxyl radical end group during the quaternization procedure (100 °C, 7 h).

II.2. Copolymer Scattering and Water Content Measurements. Copolymer Sample Preparation. Dilute solutions of the diblock copolymers were prepared at 0.70 wt % by mass in the chosen solvent. For SANS and DLS experiments, hydrogenated toluene was obtained from J. T. Baker. Deuterated toluene (d_8, Cambridge Isotopes Laboratories, D 99.6%) was used for the SANS experiments. All solvents were used as received for the preparation of the scattering samples unless otherwise noted. Before study, samples were allowed to equilibrate overnight and were studied within a few days of preparation. Some samples required stirring and mild heating to achieve complete dissolution. Once the polymers were dissolved, they formed clear solutions that were typically colorless, while a few exhibited a faint blue hue characteristic of colloidal solutions. We denote samples prepared without the addition of water as ambient samples. Water saturated samples (which we denote as saturated samples) were prepared by adding an excess of Milli-Q deionized water (~50 μL of water per each gram of polymer solution) to ambient samples using a micropipet. We then applied mild heating and agitation to the samples to facilitate the incorporation of the water until the samples became clear. Once clarified, the water saturated polymer solution was removed from the excess water. We found that the water saturated samples remained clear with no evidence of polymer precipitation or phase separation for the duration of our studies.

DLS Data Collection and Analysis. In small-angle scattering, the independent variable is the momentum transfer, q, defined as $q = (4\pi/\lambda)\sin(\theta/2)$, where λ is the wavelength of light in the medium and θ is the scattering angle. For each sample, the data was collected at seven scattering angles from 30 to 150° in 20° steps. To ensure the solutions were dust free, the sample vials were thoroughly cleaned and rinsed with filtered solvent and each sample was prepared with filtered solvent. The samples were passed through a 0.2 μm inorganic membrane filter (Whatman Anotop) directly into the scattering vial for study. All data were taken at a fixed temperature of 25 °C maintained by a circulating temperature bath. The light source for the experiments was a Coherent DPSS 500 mW laser at a wavelength of 532 nm where the laser power was attenuated as needed for each sample. We obtained the autocorrelation data using an ALV/DLS/SLS-5000 instrument with ALV-5000/E/WIN multiple τ digital realtime correlator software. Our data analysis was performed with the ALV-NonLin routines that employ a constrained regularization method fitting an integral model function to the autocorrelation data to give values of the decay time, τ. This procedure to obtain τ is similar to the CONTIN methods given by Provencher.[38]

From our analysis of the autocorrelation data, we obtained a single dominant τ, indicating a unimodal distribution of particles. The decay rate, Γ, is given as the inverse of τ and can be related to the translational diffusion coefficient of the particles, D_T, through the expression $\Gamma = D_T q^2$. Thus, we plot Γ versus q^2 to obtain a line with a slope equal to D_T. Our plots of Γ versus q^2 were linear with intercepts of nearly zero. From D_T, we can determine the hydrodynamic radii, R_h, of the diblock copolymer micelles by approximating the particles as effective, noninteracting spheres. Through the Stokes−Einstein relationship, D_T is related to R_h, $D_T = kT/(6\pi\eta R_h)$, where k is the Boltzmann constant, T is the temperature, and η is the solvent viscosity.

Neutron Contrast Matching. In neutron scattering, we use contrast matching to isolate features of selectively deuterated structures.[39] This is achieved because hydrogen and deuterium have very different neutron scattering length densities (SLDs, denoted ρ_i for component i) characterizing the way they interact with neutrons. In our SANS experiments, we consider the neutron contrast, $(\Delta\rho)^2$, defined as the square of the difference in the SLDs of two components (e.g., for components A and B, $(\Delta\rho)^2$ is equal to $(\rho_A - \rho_B)^2$). The SLD of a mixture is a weighted average of the SLDs of the individual components on a volume fraction basis, allowing the SLD of an isotopically mixed system to be determined.

In our case, we selectively deuterate the *d,h*-PS block to provide neutron contrast between it and the IL block. The amount of deuteration in the *d,h*-PS block was chosen such that its overall SLD is equal to that of d_8-toluene. Thus, when micelles are formed in d_8-toluene, there is no neutron contrast between the micelle shell comprising the *d,h*-PS chains and the d_8-toluene solvent, so we observe only the scattering from the micelle core containing the IL blocks. We refer to this contrast condition as *shell match*. Conversely, we can use a mixture of d_8- and h_8-toluene to tune the SLD to that of the IL blocks that form the micelle core. We call this contrast condition *core match*, where only the scattering from the *d,h*-PS chains that comprise the micelle shell is observed. By collecting scattering profiles in both core and shell match neutron contrasts, we can directly resolve the features of the micelle core and shell independently.

SANS Data Collection and Reduction. We performed our SANS experiments on the 30 m instrument (NG3) at the National Institute of Standards and Technology (NIST) Center for Cold Neutron Research (Gaithersburg, MD). A neutron wavelength of $\lambda = 6$ or 8 Å with a wavelength spread of $\Delta\lambda/\lambda = 0.150$ was chosen for these experiments. The scattering samples were contained in 1, 2, or 4 mm cells provided by NIST with fresh quartz windows (Esco Products). For all SANS experiments, the temperature was maintained at 25 °C.

To obtain the range of the momentum transfer, q, containing all the desired features in the scattering profiles, we used three sample-to-detector (S−D) distances of 13.1, 5.0, and 1.3 m, where the detector was offset from the center by 20 cm at the shortest

(38) Provencher, S. W.; Hendrix, J.; Demaeyer, L.; Paulussen, N. *J. Chem. Phys.* **1978**, *69*, 4273−4276.

(39) Higgins, J. S.; Benoît, H. C. *Polymers and Neutron Scattering*; Clarendon Press: Oxford, U.K., 1994.

S−D distance to give a larger q range. These three S−D distances used with 6 Å neutrons yielded a q range of 0.0040−0.4000 Å^{-1}. A special configuration available on the NG3 SANS instrument at NIST employs focusing lenses to provide a smaller incident neutron beam that consequently allows the use of a smaller beam stop, permitting collection of data at lower q values. We use this special configuration at 13.1 m with 8 Å neutrons to extend the low-q range to 0.0001 Å^{-1} to study copolymer *d*,*h*-PS(125)−IL(46).[40] The two-dimensional intensity data were corrected and averaged to obtain one-dimensional data on an absolute scale using data correction and reduction routines developed at NIST.[41] The contribution to the scattering profile due to the sample cell is removed from the one-dimensional data obtained using the reduction procedures provided by NIST, and solvent scattering is directly subtracted from the one-dimensional profiles on a volume fraction basis. We note that the magnitude of the scattering signal from the copolymer micelle samples greatly exceeds the solvent scattering in all but the highest-q regime. In a few cases, we see a slight upward trend in the lowest-q data points of the SANS profiles, particularly those in the shell match solvent. We attribute these points to larger structures, perhaps small amounts of emulsified water (which would only be evident in the shell match solvent due to the neutron contrast). Consequently, these data do not provide information about the micelle structures and we eliminate these points from our analysis.

Once the data has been properly corrected and normalized, we obtain the macroscopic differential scattering cross section, $d\Sigma/d\Omega$ (q). For a dilute solution of noninteracting identical particles, $d\Sigma/d\Omega$ (q) can be expressed as[42]

$$\frac{d\Sigma}{d\Omega}(q) = NV^2(\Delta\rho)^2P(q) + B \qquad (1)$$

In this expression, N is the number density of scattering centers, V is the volume of a scattering center, $P(q)$ is the form factor, and B is the incoherent background. The intensity profile of the form factor is created by the interference effects within an individual scattering center and thus gives information about the size and structure of the scattering centers. Analytical expressions are available for the form factors of shapes commonly encountered in small-angle scattering.[21,22] We will consider some of these expressions in our analysis in addition to evaluating their asymptotic behavior. We note that, for our dilute solution studies, we do not consider the effects of interactions between particles and thus do not include the structure factor in eq 1. The incoherent scattering, given by B, gives no structural information about the sample and is treated as a uniform background contribution to the scattering intensity.

Karl Fischer Water Content Testing. We quantify the trace amounts of water present in our system with Karl Fischer titration. The preparation of the saturated samples is detailed above. We additionally prepared both ambient and saturated h_8-toluene samples in the same fashion to determine the water levels in our solvent. The Karl Fischer titration analysis of the samples was performed by Galbraith Laboratories (Knoxville, TN).

III. Results

Scattering profiles of elongated structures can provide a wealth of information about the shape and flexibility of the structures.[43−45] On the basis of the length scales probed (i.e., the q range considered), an elongated micelle can show properties of a semiflexible wormlike chain, rigid rod, or effective sphere. In Figure 1, the SANS profiles illustrate differences due to the effects of neutron contrast, IL block length, and water saturation. Through the appropriate representation of the scattering data in each q regime, we can extract detailed information about the micelle dimensions and structure.

In the low-q limit, we determine the micelle radius of gyration (R_g) of both the core and shell of the micelle using the SANS data taken at the two contrast conditions of shell and core match. Due to the large length scales probed in this regime, we can employ the Guinier approximation where, in the limit of small qR_g, the form factor is approximated as[46]

$$P(q, R_g) \approx \exp\left(-\frac{(qR_g)^2}{3}\right) \qquad (2)$$

Hence, a Guinier plot (ln[$d\Sigma/d\Omega$ (q)] vs q^2) should be linear in the low-q limit with a slope of negative $R_g^2/3$ and an intercept that contains information about the aggregation number, N_{agg}, and micelle molar mass, $MW_{micelle}$. Our Guinier plots for the sample prepared under ambient conditions are linear, and the data obtained from these plots including the $R_{g,core}$, $R_{g,shell}$, N_{agg}, and $MW_{micelle}$ values are given in Tables 2 and 3. The SANS data of the saturated samples are treated in the same manner, and the $R_{g,core}$ and $R_{g,shell}$ data are given in Table 4. The data obtained from DLS can also be considered with the SANS low-q data, and thus, the R_h values are also presented in Table 2.

At intermediate length scales (i.e, $qR_g > 1$), we begin to probe the micelle flexibility and cross-sectional dimensions. The expression for the form factor for an infinitely thin rod can be modified with a Guinier-like factor to account for the finite cross section of a wormlike chain[42]

$$\frac{d\Sigma}{d\Omega}(q) = NV^2(\Delta\rho)^2P(q)_{rod} \approx \pi NV^2(\Delta\rho)^2\left(\frac{1}{qL}\right)\exp\left(-\frac{R_{g,xs}{}^2q^2}{2}\right) \qquad (3)$$

where L is the length of the micelle and $R_{g,xs}$ is the cross-sectional radius of gyration of the wormlike chain. Thus, a Kratky−Porod wormlike chain plot of ln[$d\Sigma/d\Omega$ (q) × q] versus q^2 will be linear at intermediate q values for structures with characteristics of wormlike chains. By fitting a line to this region of the data, we can obtain the $R_{g,xs}$ value from the slope. Our scattering data for the copolymers in shell match solvent all exhibit a linear regime at intermediate q, as shown in Figure 2, and the $R_{g,xs}$ data for the micelle core are obtained from the linear fits, as given in Table 2 for the ambient samples. This analysis is also applied to the saturated samples, and the associated $R_{g,xs}$ values are given in Table 4.

At large q values, the length scales we are investigating are small and locally the micelles appear as rigid rods. In the limit of an infinitely thin rod at large q, the form factor approaches the asymptotic value[45]

$$P(q)_{rod} \approx \frac{\pi}{qM_L} \qquad \text{at large } q \qquad (4)$$

where M_L is the mass per unit length of the rod. At lower q values, large distances are probed and the elongated micelles may appear flexible like a Gaussian coil. For a

(40) Choi, S. M.; Barker, J. G.; Glinka, C. J.; Cheng, Y. T.; Gammel, P. L. *J. Appl. Crystallogr.* **2000**, *33*, 793−796.
(41) *SANS Data Reduction and Imaging Software*; Cold Neutron Research Facility, NIST: Gaithersburg, MD, 1996.
(42) King, S. M. In *Modern Techniques for Polymer Characterisation*; Dawkins, J. V., Ed.; John Wiley & Sons Ltd: New York, 1999; pp 171−232.
(43) Casassa, E. F. *J. Chem. Phys.* **1955**, *23*, 596−597.
(44) Holtzer, A. *J. Polym. Sci.* **1955**, *17*, 432−434.
(45) Denkinger, P.; Burchard, W. *J. Polym. Sci., Part B: Polym. Phys.* **1991**, *29*, 589−600.
(46) Glatter, O.; Kratky, O. *Small Angle X-ray Scattering*; Academic Press: London, 1982.

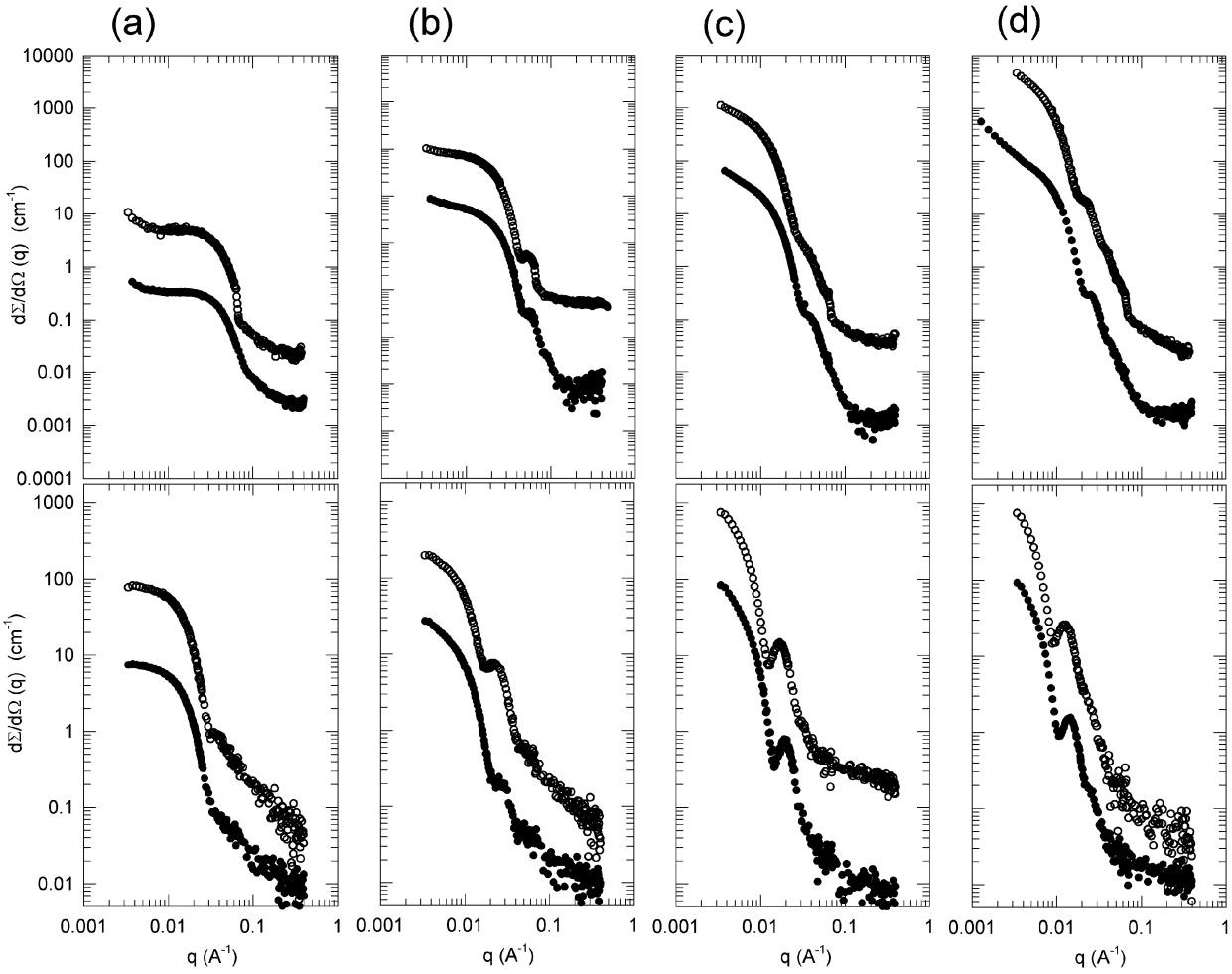

Figure 1. The SANS scattering profiles are shown for copolymers (a) PS(125)−IL(7), (b) PS(125)−IL(18), (c) PS(125)−IL(33), and (d) PS(125)−IL(46) at 0.7 wt % in shell match d_8-toluene (upper row) and core match h_8/d_8-toluene (lower row). Each graph shows the samples prepared at ambient (closed circles) and saturated (open circles) conditions, where the data for the saturated samples are offset by a factor of 10 for clarity. The error bars for the data sets are typically the size of the points in the low-q regime and within the spread of the data in the high-q regime.

Table 2. Structure and Flexibility of Ambient *d,h*-PS(125)−IL Copolymer Micelles Obtained from Scattering Analyses[a]

	IL core						*d,h*-PS shell			micelle
copolymer	$R_{g,core}$ (Å)	$R_{g,xs}$ (Å)	L (Å)	$L/2R_{g,xs}$	l_p (Å)	L/l_p	$R_{g,shell}$ (Å)	t_{shell} (Å)	$\phi_{d,h-PS}$	R_h (Å)
d,h-PS(125)−IL(7)	31 ± 2	21 ± 1	97 ± 8	2.4	24 ± 3	4.0	108 ± 1	103 ± 3	0.04	181 ± 12
d,h-PS(125)−IL(18)	87 ± 1	60 ± 1	264 ± 1	2.2	41 ± 2	6.9	195 ± 1	148 ± 1	0.07	372 ± 13
d,h-PS(125)−IL(33)	151 ± 1	98 ± 1	467 ± 1	2.4	55 ± 3	8.5	320 ± 1	230 ± 2	0.08	755 ± 8
d,h-PS(125)−IL(46)	226 ± 1	149 ± 1	692 ± 3	2.3	95 ± 10	7.3	380 ± 2	214 ± 3	0.11	858 ± 24

[a] Error margins are rounded up to the nearest angstrom.

Table 3. Assembly Properties of Ambient *d,h*-PS(125)−IL Copolymer Micelles

copolymers	N_{agg}	$MW_{micelle}$ (g /mol)	error (%)
d,h-PS(125)−IL(7)	26	4.15×10^5	10
d,h-PS(125)−IL(18)	235	4.46×10^6	1
d,h-PS(125)−IL(33)	606	1.41×10^7	2
d,h-PS(125)−IL(46)	1503	4.06×10^7	1

Gaussian coil, the form factor tends to a different asymptotic value at large q[45]

$$P(q)_{coil} \approx \frac{6}{q^2 l_p M_L} \qquad \text{at large } q \qquad (5)$$

where l_p is the persistence length of the coil. Structures may exhibit both the rod and coil form factors on different length scales or q regimes. For these structures, the transition between these two regimes occurs at a q value equal to q^* determined by equating eqs 4 and 5 to obtain $l_p = 6/(\pi q^*)$.[45] This q^* value can be determined by plotting the data in a bending rod (BR) plot, thus allowing determination of the micelle flexibility as characterized by l_p. In a BR plot, $q \times d\Sigma/d\Omega\ (q)$ is plotted versus q.[45] If the crossover from coil to rod behavior exists, there will be a downward trend in the scattering profile ($q \times d\Sigma/d\Omega\ (q) \sim q^{-1}$) followed by a plateau ($q \times d\Sigma/d\Omega\ (q) \sim q^0$), where the transition between these features occurs at q^*.[45] The abscissa in a BR plot can be normalized by R_g to emphasize the effects of polydispersity.[45] We plot our data for both the ambient and saturated copolymers in shell match solvent as a BR plot (Figure 3) and a normalized BR plot (Figure 4). For the all of the copolymers, the transition from q^{-1} scaling to the plateau regime is clearly evident, allowing us to locate q^* from these plots. The values of l_p

Table 4. Structure and Flexibility of Water Saturated *d,h*-PS(125)−IL Copolymer Micelles Obtained from Scattering Analyses[a]

	IL core						*d,h*-PS shell	
copolymer	$R_{g,core}$ (Å)	$R_{g,xs}$ (Å)	L (Å)	$L/2R_{g,xs}$	l_p (Å)	L/l_p	$R_{g,shell}$ (Å)	t_{shell}* (Å)
d,h-PS(125)−IL(7)	32 ± 3	24 ± 1	94 ± 11	2.7	24 ± 3	5.4	110 ± 1	93 ± 3
d,h-PS(125)−IL(18)	82 ± 1	64 ± 1	237 ± 3	1.9	41 ± 2	5.8	197 ± 1	156 ± 2
d,h-PS(125)−IL(33)	162 ± 1	113 ± 1	488 ± 1	2.2	55 ± 3	8.8	316 ± 1	211 ± 2
d,h-PS(125)−IL(46)	239 ± 1	168 ± 1	718 ± 1	2.9	95 ± 10	10.4	418 ± 2	156 ± 3

[a] Error margins are rounded up to the nearest angstrom.

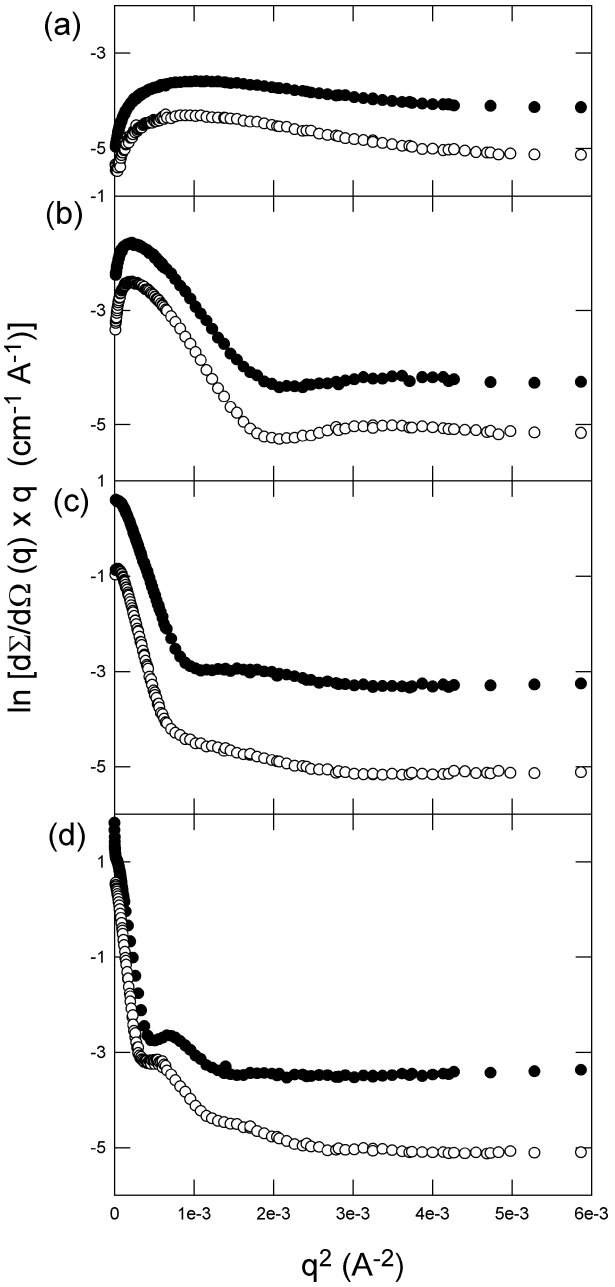

Figure 2. The SANS data are displayed as a Kratky−Porod wormlike chain plot for the 0.7 wt % copolymer solutions in shell match d_8-toluene prepared under ambient (closed circles) and saturated (open circles) conditions for copolymers (a) PS(125)−IL(7), (b) PS(125)−IL(18), (c) PS(125)−IL(33), and (d) PS(125)−IL(46). The ambient data are offset by an additive factor for clarity of (a) 1, (b) 1, (c) 2, and (d) 2.

obtained from this analysis are given in Tables 2 and 4 for the ambient and saturated samples, respectively.

Another means to study the crossover from wormlike to rodlike behavior at intermediate q values is the Kratky plot, where we plot $q^2 \times d\Sigma/d\Omega$ (q) versus q.[42] In this representation, Gaussian coil behavior is indicated by a plot that levels off to reach a asymptotic behavior at high q.[39] In contrast, the Kratky plot for a rodlike particle will show a consistent linear rise with increasing q due to the non-Gaussian perturbations of the structure.[45] For star and ring polymers, a low-q peak indicating the compactness of these structures is seen in their Kratky plots.[39] Our Kratky plots of the PS−IL micelles show very interesting behavior with all three of the following distinctive features present in the plots: a low-q peak, a plateau at intermediate q, and a linear rise at high q (Figure 5).

IV. Discussion

IV.1. Micelle Core and Shell at Ambient Conditions: Shape and Flexibility. Our SANS analysis provides detailed information about the shape and flexibility of the micelle core and shell. In shell match toluene, we observe the features of the micelle core, as shown by the scattering profiles of the four copolymers in the upper row of Figure 1. For the samples prepared at ambient conditions, we see that with increasing IL block length (N_{IL}) the magnitude of the scattering profiles at low q increases dramatically. Following from eq 1, this indicates that the volume of the micelles, or micelle dimensions, are increasing with N_{IL}. We also see that the features in the scattering profile due to the form factor become more prominent with increasing N_{IL}, including a distinct inflection in the intermediate-q regime.

In our prior studies of an analogous fully hydrogenated PS−IL system, we considered several model form factors in detail to determine the most accurate characterization of the micelle morphology.[27] Specifically, we found that our micelle form factor was not consistent with that of a monodisperse or polydisperse core−shell sphere, as we could only fit either the low- or high-q regimes. On the basis of the features of the SANS scattering profiles, we considered the possibility of elongated micelle structures and found excellent agreement of our data to the form factor of a core−shell cylinder.[27] As our prior studies on the fully hydrogenated systems suggested the formation of cylindrical elongated micelles,[27] we apply both the Kratky−Porod wormlike chain and BR plot analyses to our shell match data where we are viewing the micelle core. The Kratky−Porod analyses for all four of the copolymers show the linear regime at intermediate q expected for semiflexible elongated structures. The slope of the linear regime becomes steeper with increasing N_{IL}, indicating the micelle core cross section grows with the IL block length. Furthermore, the location of the linear regime shifts to lower q with increasing N_{IL}, again indicating that the features of the semiflexible elongated structures are seen at larger lengths scales for longer core-forming blocks.

In our BR plot analysis, we observe the crossover from rodlike to wormlike behavior of the elongated structures by the presence of a q^{-1} scaling regime followed by a

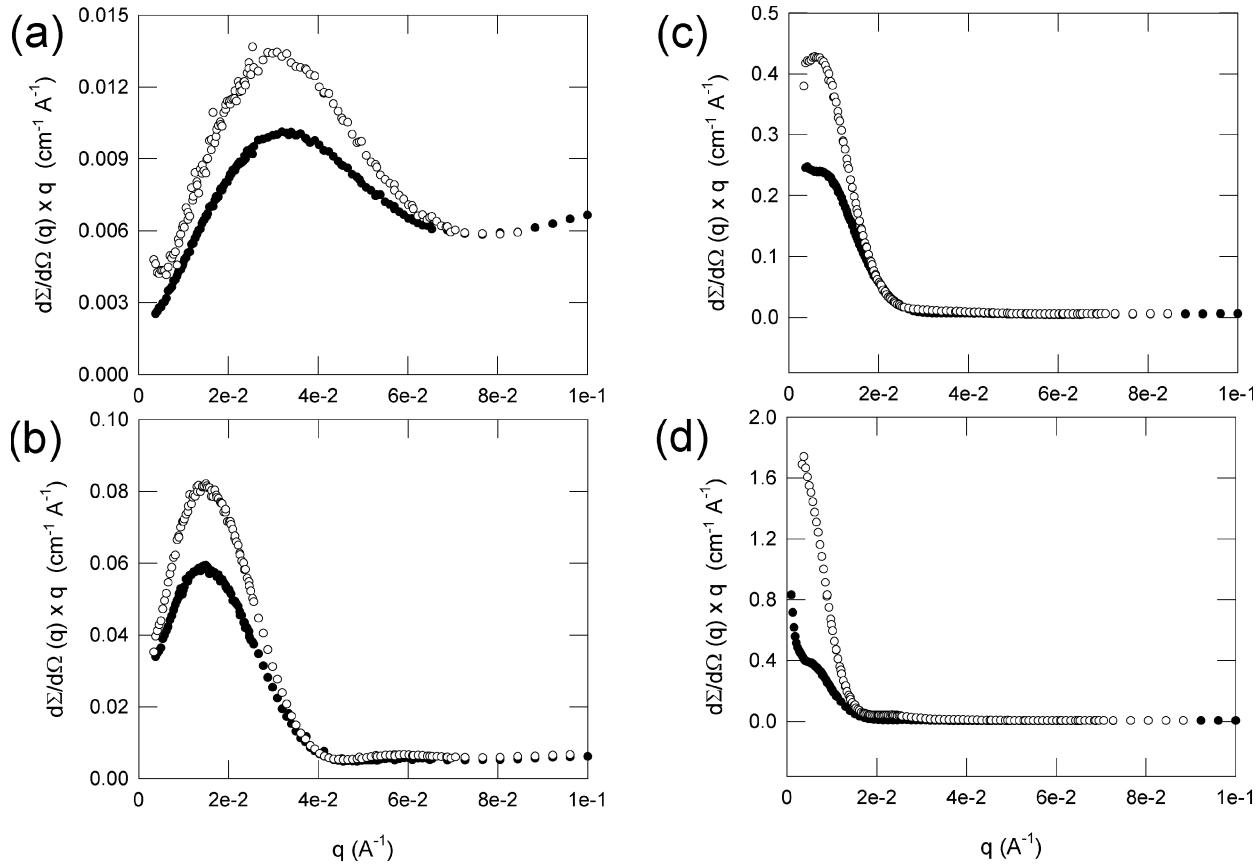

Figure 3. The SANS data are displayed as bending rod (BR) plots for the 0.7 wt % copolymer solutions in shell match d_8-toluene prepared under ambient (closed circles) and saturated (open circles) conditions for copolymers (a) PS(125)−IL(7), (b) PS(125)−IL(18), (c) PS(125)−IL(33), and (d) PS(125)−IL(46).

plateau in the plots, as shown in Figure 3. These features in a BR plot indicate the elongated micelles have characteristics of wormlike chains (i.e., semiflexible elongated structures). The persistence length, l_p, is determined by the q value, q^*, where the q^{-1} regime ends and the plateau regime begins. We find that l_p increases with N_{IL}, indicating that the micelles become less flexible as their cross sections grow. By normalizing the abscissa by $R_{g,core}$, we find that the positions of the peak or inflection for each copolymer in the series nearly coincide at a $qR_{g,core}$ value of 1.4, as shown by the reference line in Figure 4. This peak position is significant, as it is expected for monodisperse chains,[45] indicating not only that our micelles are relatively monodisperse in cross section, as dictated by the IL block length, but also that the thermodynamics of assembly may drive them to a uniform aspect ratio as well. This is further supported by the undulations in the plateau region at higher $qR_{g,core}$ values that are characteristic of monodisperse rigid objects.[45]

From the Guinier and Kratky−Porod wormlike chain analyses, we obtain the ambient micelle dimensions given in Table 2 and plotted in Figure 6. Assuming the micelles are rodlike such that $R_{g,core}$ is approximated as $R_{g,rod}$ and taking the cross-sectional radius of the rod, R_{xs}, as $R_{g,xs}$, we use the following expression for a rod to determine the length of the micelles, L.

$$R_{g,rod}^2 = \frac{L^2}{12} + \frac{R_{xs}^2}{2} \qquad (6)$$

We find that all the dimensions of the micelle core, including $R_{g,core}$, $R_{g,xs}$, and L, are linear functions of N_{IL}, consistent with our previous study.[27] This finding is not typical for copolymer micelles and has interesting implications for the structure of the IL chains comprising the core. From a linear least-squares fit to the data, we find that $R_{g,xs}$ (in angstroms) = 3.5 Å × N_{IL}. This linear relation suggests a Flory exponent of 1 (i.e., a fully extended chain conformation) for the IL block. While this fully extended chain conformation is not expected, it can be rationalized by the strong interactions between closely packed charged polymer blocks in the micelle core. The increase in the micelle cross section by 3.5 Å for each additional IL unit added to the block is consistent with the length anticipated for the polymer backbone of a fully extended IL unit (i.e., about twice the C−C single bond length, 3.1 Å). Considering the packing of extended chains, the micelle may not adopt a circular cross section; different cross-sectional packing arrangements, such as ellipsoidal or tablet-shaped configurations, would allow for more efficient packing of the IL blocks, as illustrated schematically in Scheme 2. Our earlier SANS studies on fully hydrogenated PS−IL systems showed good agreement with a cylindrical micelle form factor, leading us to conclude that any deviation from a circular cross section of the micelle core is not considerable.[27] Additional analyses and computational methods allow detailed characterization of micelle cross sections from scattering data and have shown promise in their use for small molecule surfactant elongated micelles.[23,47,48] We did not employ further analysis of these structures to explore their cross-sectional profile in more detail due to the large number of parameters needed to fit the data.

(47) Garamus, V. M.; Pedersen, J. S.; Maeda, H.; Schurtenberger, P. *Langmuir* **2003**, *19*, 3656−3665.
(48) Bergström, M.; Pedersen, J. *J. Phys. Chem. B* **1999**, *103*, 8502−8513.

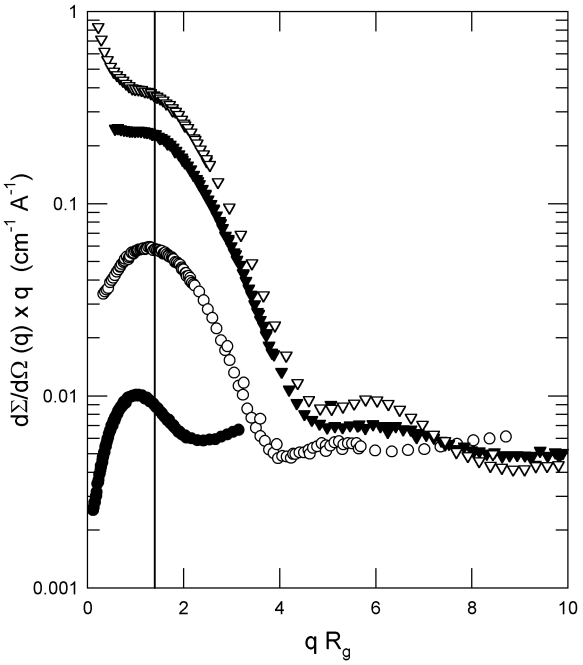

Figure 4. The data for the 0.7 wt % ambient copolymer solutions in shell match d_8-toluene of PS(125)−IL(7) (closed circles), PS(125)−IL(18) (open circles), PS(125)−IL(33) (closed triangles), and PS(125)−IL(46) (open triangles) are displayed as a bending rod (BR) plot where the abscissa is nondimensionalized with the $R_{g,core}$ values determined by the Guinier analysis (Table 2). A reference line at a qR_g value of 1.4 shows the peak position anticipated for a monodisperse wormlike chain.

Furthermore, we were not confident that the potential deviations would be large enough to distinguish conclusively from such fits.

The increase in the micelle cross section per IL repeat unit slightly exceeds the expected extended length for the IL unit, indicating that there may be a void in the center of the structures to relieve some of the packing constraints. The presence of a cavity in an elongated micelle structure has been observed by TEM in block copolymer micelles of poly(ferrocenylsilane)−poly(dimethylsiloxane) (PFS−PDMS).[49] The possible presence of a hollow cavity in our micelles has direct implications on the ability of these systems to solubilize guest molecules and may make them attractive candidates for templating or nanoreactor applications.

The linear relationship between the micelle core length and IL block length indicates the micelles have an equilibrium length determined by their composition. In many elongated micelle systems, the cross-sectional dimensions of the micelles are determined by the properties of the assembling molecules, but the length may be highly polydisperse. There is evidence in our BR plots that our systems form relatively monodisperse micelles, and this relation between L and N_{IL} further supports this conclusion. This link between L and N_{IL} may be due to the balance between favorable packing of the IL blocks forming the micelle core and the PS chain conformation of the surrounding shell. While the extended IL chains of the core tend to pack into micelle structures that minimize the curvature of the interface formed between the IL core and PS shell, the PS chains favor formation on a curved interface to allow for more expanded conformations that minimize chain−chain interactions. Thus, a balance between these states may govern micelle length, which will have curved interfaces at its end with flatter interfaces along its length.

Comparing the various micelle dimensions presented in Table 2, we can infer more about their structures. We see that the cores of the elongated structures show a relatively constant aspect ratio of ∼2.3. We also find that there are four to eight persistence lengths per a micelle core, where the number of persistence lengths increases with the ionic liquid block length and seems to plateau for the larger IL blocks. These findings indicate that the

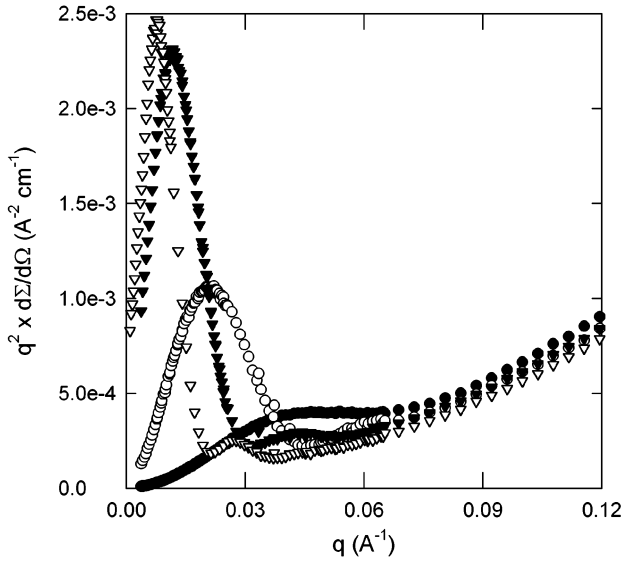

Figure 5. The data for the 0.7 wt % ambient copolymer solutions in shell match d_8-toluene of PS(125)−IL(7) (closed circles), PS(125)−IL(18) (open circles), PS(125)−IL(33) (closed triangles), and PS(125)−IL(46) (open triangles) are displayed in a Kratky plot.

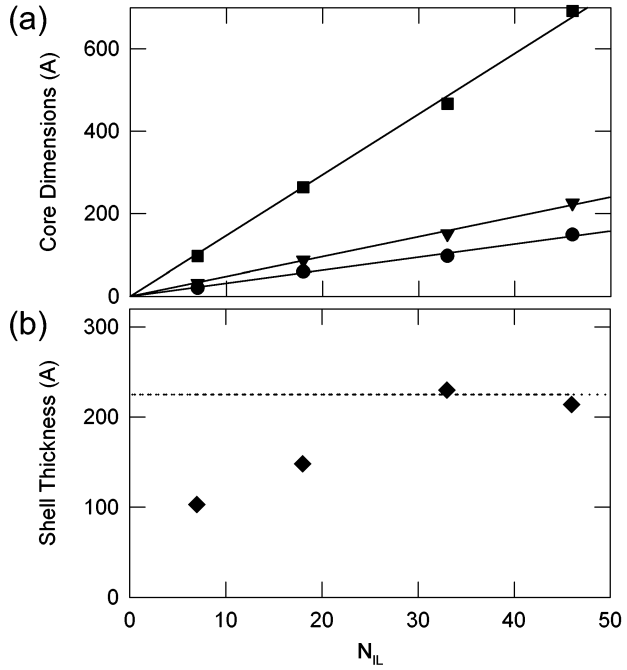

Figure 6. The micelle dimensions of copolymers prepared at ambient conditions are shown as a function of the IL block length, N_{IL}. In part a, the dimensions of the micelle core are shown along with the respective linear least-squares fits, L (squares), $R_{g,core}$ (triangles), and $R_{g,xs}$ (circles). In part b, the shell thickness (diamonds), t_{shell}, is shown as a function of N_{IL}, where the dashed line shows the apparent plateau of the data.

(49) Raez, J.; Barjovanu, R.; Massey, J. A.; Winnik, M. A.; Manners, I. *Angew. Chem., Int. Ed.* **2000**, *39*, 3862.

Scheme 2. Schematic Illustration of the Possible Assembly Structures of the (a) PS−IL Elongated Micelles with (b) Circular, (c) Ellipsoidal, or (d) Tablet-Shaped Cross Sections

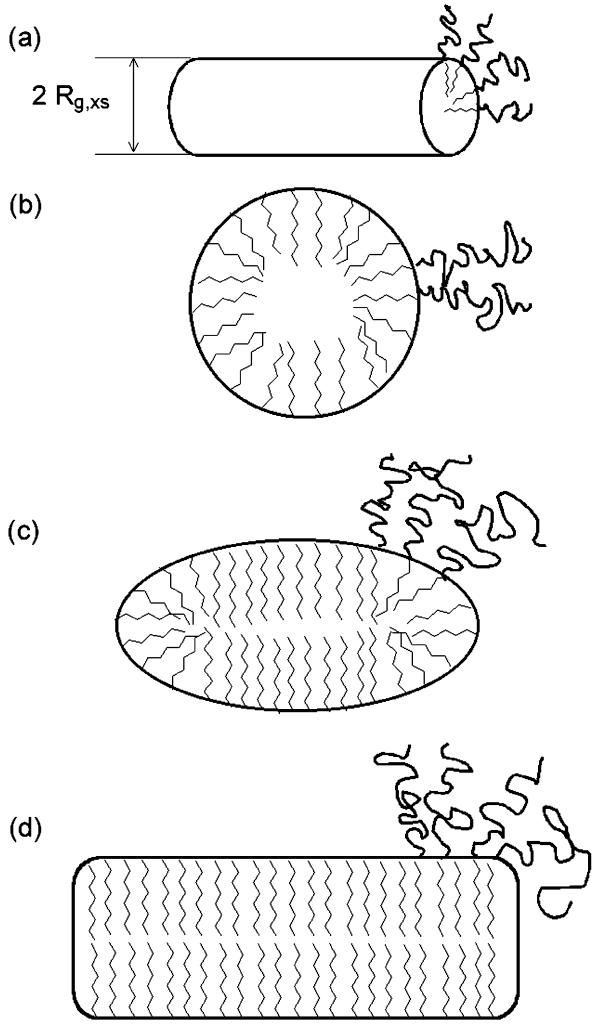

ambient micelle core structures are relatively short and semiflexible cylindrical structures.

With our SANS data taken in core match conditions, we can assess the properties of the micelle shell. Qualitatively, the features of the scattering patterns become more distinct with increasing IL block length. In particular, an inflection or peak develops in the intermediate-q regime, which is due to the "hole" in the shell created by the contrast matched micelle core, while the high-q scattering shows the linear power-law behavior due to the scattering from the PS chains comprising the shell. We again use the Guinier approximation in the low-q regime to obtain $R_{g,shell}$ and define the effective shell thickness, t_{shell}, as the difference between the overall radius of the shell and core, which we determine from the respective R_g values.

Our results show that the shell thickness grows with the IL block length, although not linearly, as the shell thickness seems to reach a plateau with increasing IL block length (Figure 6). As the size of the core increases with N_{IL}, the curvature of the core−shell interface is reduced. The chain conformation on the highly curved interface of a small core is starlike. In contrast, the chains adopt a brushlike conformation on the locally flat interface of a large core. In this dense brushlike configuration, the chains are extended and stretched from the surface to avoid the unfavorable chain−chain interactions characterized by a blob size that remains constant with radial distance from the core. The starlike conformation leads to local chain stretching very close to the core−shell interface but with blob sizes that increase with radial distance from the core such that the ends of the chains are almost in a dilute-solution-like conformation. This starlike conformation is a thermodynamically more favorable state for the PS chains. Thus, the energetic penalty paid for PS chain stretching in the dense brushlike shell is balanced by a more favorable packing arrangement of the IL chains in the micelle core.

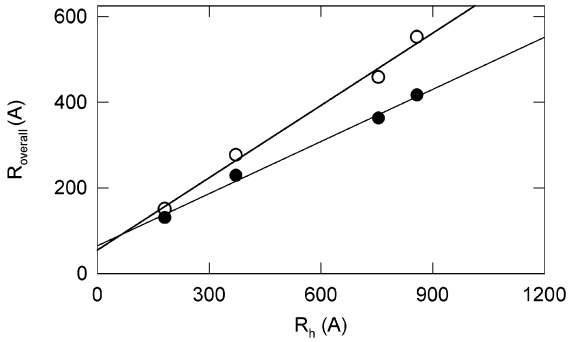

Figure 7. The DLS hydrodynamic radius, R_h, for the copolymer micelles in toluene is compared to the overall cross-sectional radius (closed circles) and the overall length radius (open circles) calculated from the micelle dimensions obtained with the SANS analyses. Linear fits to the data are shown with solid lines.

From our Guinier analyses, we can estimate the volume fraction of highly swollen PS in the shell, $\phi_{d,h-PS}$, using the value of the scattering intensity as q approaches zero ($d\Sigma/d\Omega$ ($q \rightarrow 0$)) from both the core and shell match conditions. We find $\phi_{d,h-PS}$ to be <0.12 in all cases. The $\phi_{d,h-PS}$ value increases with N_{IL}, consistent with our interpretation that the PS chain conformations move from starlike to brushlike as the core curvature changes with growing N_{IL}.

To complement the characterization of the micelle dimensions conducted with SANS, we study the ambient micelle solutions using DLS. Since DLS is not sensitive to deuterium labeling, we probe the entire micelle structure with this technique. From DLS, we measure the hydrodynamic radius, R_h, which is a measure of the average of the overall radius of the entire micelle. Here, we find that R_h does not vary linearly as N_{IL} does; while the dimensions of the micelle core are linearly related to N_{IL}, the radii measured here additionally include the PS shell thickness, which is affected by the size of the core and the curvature of the core−shell interface. To assess the consistency between the results obtained from SANS and DLS, we compare R_h to the overall radii anticipated from the dimensions obtained from SANS. In particular, our SANS results yield two overall radii, one for the overall length ($R_{overall,L} = t_{shell} + L/2$) and one for the overall cross section ($R_{overall,xs} = t_{shell} + R_{xs}$). We see the R_h values correlate linearly with both $R_{overall,L}$ and $R_{overall,xs}$, as shown in Figure 7. We find R_h is consistently larger than the calculated SANS overall radii. This is due to the fact that the entire diffuse micelle shell is viewed by DLS, whereas the SANS measurements tend to underestimate the shell size. The volume fraction of PS becomes extremely low with radial distance from the micelle core, and the SANS technique is not sensitive to the small contrast created by these dilute chains and thus yields a smaller shell size. The direct correlation between the results obtained by the two different techniques corroborates the micelle dimensions.

Returning to the SANS analysis for our ambient shell match samples, we view the data in the Kratky representation (Figure 5). Our plots have three distinctive features: a low-q peak, a plateau at intermediate q, and a linear rise at high q. Qualitatively, we find the low-q peak shifts to lower q with increasing IL block length, indicating the feature is due to larger scale structures with growing N_{IL}. We find the location of this peak to be at a qR_g value of 1.3−2.0, similar to values found for star polymers[50] and dendrimers,[51] indicating that the micelle core has a compact nature. In our system, extended IL blocks emanating outward from the center of the micelle cross section give rise to a compact core. The plateau in our plots indicates that, at the intermediate length scales, the elongated micelles behave like coils.[39,45] At larger q, the dimensions we are probing include length scales smaller than $2l_p$ and thus the micelles appear stiff, leading to the linear rise in the Kratky plot at high q characteristic of rodlike systems.[39,45] The location of the plateau region that occurs following the low-q peak and just before the high-q rise should be inversely proportional to the persistence length of the structures (i.e., a ql_p value of 0.25−1.5).[39] We find that the inverse of the q value locating this plateau regime is linearly related to the IL block length for this series, indicating that the relationship between the upturn in the Kratky plot is in fact due the semiflexible nature of the elongated micelles. However, we do not define the persistence length from this location, as this method is not as robust as the BR plot method for obtaining the persistence length.

IV.2. Micelle Aggregation. While we have discussed the shape of the micelles, we now consider the aggregation behavior that drives their formation. Generally, the self-assembly or aggregation of copolymers to form micelle structures in a selective solvent is driven by thermodynamics; the entropy cost for forming organized structures is outweighed by the more favorable energetic state that results as the insoluble blocks are shielded from the solvent environment. To allow for a richer understanding of the assembly behavior, many researchers have studied the dependence of micelle formation on the lengths of both the insoluble and soluble blocks. One parameter that is used to quantify the self-assembly behavior is the aggregation number, N_{agg}, or the number of copolymers that come together to form each micelle assembly. Generally, it has been found that the expressions relating the block lengths of the insoluble and soluble blocks (N_I and N_S, respectively) to the aggregation number follow a power-law behavior ($N_{agg} \sim N_I^{\alpha} N_S^{\beta}$).[52] Typically, the association leads to a core with liquidlike or globulelike properties, and theory and experiment have found $\alpha = {}^4/_5$ such that $N_{agg} \sim N_I^{4/5}$.[53] In the event that the cores are not liquid but rather glassy or crystalline, the aggregation behavior may be significantly altered.

To determine N_{agg}, we assume that each IL repeat unit will have a fixed volume, v_{IL}, that contributes to the total core volume, V_{core}, such that $V_{core} = N_{agg} N_I v_{IL}$. We determine V_{core} simply from geometry (i.e., $V_{core} = \pi R_{g,xs}^2 L$). We report our data for N_{agg} and for the micelle molar mass, $MW_{micelle}$, of the ambient samples in Table 3. From these data, we find that $N_{agg} \sim N_{IL}^2$ (or $\alpha = 2$), as shown in Figure 8. This scaling behavior indicates that we do not have typical liquid micelle cores. Marques' theoretical predictions for micelle associative behavior predict $\alpha = 2$ for liquid cores where there is a very large interfacial tension creating a high degree of chain deformation within the core such that the core radius scales linearly with the insoluble block length.[53] This is in complete agreement with our results where we find the core dimensions scale linearly with N_{IL} whereas N_{agg} scales with N_{IL}^2.

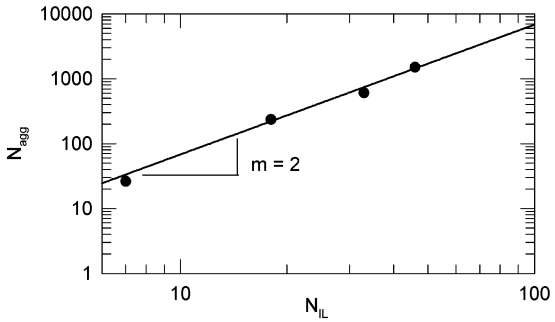

Figure 8. The micelle aggregation number, N_{agg}, is plotted against the IL block length, N_{IL}, in a double logarithmic plot. The solid line indicates a power-law fit to the data with a slope of 2.

From this aggregation data, we see that the unique self-assembly behavior of these micelles is dictated by the conformation of the IL block. The extended conformation of the IL block in turn drives the packing of the micelle core into an elongated structure. The energy gain for the extended IL blocks forming associations in the micelle core must outweigh the penalty for chain stretching of the PS shell, allowing the cylindrical structures to form. Thus, in our system, there is a link between the aggregation behavior of the copolymers and the resultant micelle morphology due to the thermodynamics of the assembly process.

Other groups observing elongated micelle structures have considered the thermodynamics of the assembly process and have postulated the energy contributions driving the formation of nonspherical assemblies. For example, Bates and co-workers have suggested that copolymer micelle morphologies should be analogous to those found in small molecule surfactants, where molecular packing and surface curvature are used to explain the thermodynamics of self-assembly.[3,13] In another example, in their studies of poly(ferrocenylsilane)−poly(dimethylsiloxane) (PFS−PDMS) and poly(isoprene)−PFS (PI−PFS), Manners and Winnik found that the morphology of their nonspherical micelles was driven by crystallization of the PFS core-forming block.[54,55] In a detailed study of the effects of sample preparation on the micelle morphology of PFS−PDMS, they found that cylindrical micelles formed when samples were prepared below the melting temperature of the core-forming block, while spherical micelles formed when prepared above this melting temperature.[55] In a related study of the PI−PFS copolymer, they looked at the effects of the block ratio on the micelle morphology and learned that the micelles formed either cylindrical or tapelike structures, or a combination of both, depending on the block ratio.[54] Thus, a combination of factors including the interactions of the core-forming block, such as crystallization, and the block ratios affected the thermodynamics of these self-assembling systems. In our system, we find that the interactions of the core-forming block dominate the association and aggregation behavior of our *d*,*h*-PS−IL

(50) Richter, D.; Farago, B.; Fetters, L. J.; Huang, J. S.; Ewen, B. *Macromolecules* **1990**, *23*, 1845−1856.
(51) LaFerla, R. *J. Chem. Phys.* **1997**, *106*, 688−700.
(52) Moffitt, M.; Eisenberg, A. *Macromolecules* **1997**, *30*, 4363−4373.
(53) Marques, C. M. *Langmuir* **1997**, *13*, 1430−1433.
(54) Cao, L.; Manners, I.; Winnik, M. A. *Macromolecules* **2002**, *35*, 8258−8260.
(55) Massey, J. A.; Temple, K.; Cao, L.; Rharbi, Y.; Raez, J.; Winnik, M. A.; Manners, I. *J. Am. Chem. Soc.* **2000**, *122*, 11577−11584.

copolymers. To learn about the nature of the IL blocks of the micelle core in more detail, we must apply other analysis methods that would probe the length scales of the associating chain structures such as wide-angle X-ray scattering (WAXS).

IV.3. Micelles Saturated with Water. The solublization of small molecules into micelle structures is necessary for many of their applications, and thus, we explore the effects of partitioning water in our micelle system. The partitioning of water into micelles structures has been explored in detail theoretically by Nagarajan[56] and experimentally by Schurtenberger,[18,26] Eisenberg,[57] and Cogan.[58] In these studies, the partitioning of water often led to changes in the micelle structures. We explore the effects of water on our micelles by studying samples of the four copolymers saturated with water in both the core and shell match solvents.

Saturation of the micelle solutions with water leads to subtle changes in the micelle structures, as seen in the SANS profiles. In the shell match scattering profiles (Figure 1), the addition of water leads to enhancement of the features in the scattering profile including a more defined intermediate-q inflection and a rise in the low-q regime. The core match scattering profiles (Figure 1) do not show a significant change in the low-q behavior with water saturation, indicating the structure and aggregation of the PS shell is not significantly altered by the presence of water. The position of the peak or inflection in these profiles shifts to a slightly lower q value when saturated with water indicating slight growth of their cores.

By analyzing the scattering data in an analogous fashion to the ambient samples, we obtain the parameters that characterize the dimensions and flexibility of the micelle structures (Table 4). The length of the micelles remains relatively unchanged with water addition; however, we find that the core cross sections of the saturated micelles are slightly larger than their ambient counterparts. From this minor cross-sectional swelling, we conclude that the packing of the IL blocks into the micelle core is not significantly altered by the presence of water and can accommodate the water without much rearrangement. Swelling of micelles upon addition of water by lengthening was observed by Schurtenberger upon addition of water to a lecithin micelle.[18,26] The properties of the PS shell of our micelles appear to be unaltered by the presence of water, as $R_{g,shell}$ is essentially the same in the ambient and saturated micelles.

The BR plots of the four saturated samples in shell match solvent all show a peak followed by a plateau, allowing determination of the persistence lengths of the elongated micelles for each copolymer. We find that the persistence length of the elongated micelles grows with the IL block length. Thus, as the cross section of the micelle increases (i.e., $R_{g,xs}$ scales linearly with N_{IL}), the micelles become stiffer. While the positions of the peak to plateau transition in the BR plots do not shift with the addition of water, we do see that the magnitude of the peak is increased in the saturated samples versus those prepared at ambient conditions. Typically, an increase in height of a BR plot peak indicates that the number of persistence lengths comprising the elongated structure increases.[45,59] As the flexibility of our micelles (given by l_p) does not change with the addition of water nor does their length, we conclude the change in peak height is due to the enhanced neutron contrast of the micelle cores containing water.

Table 5. Water Content in Saturated *d,h*-PS(125)−IL Copolymer Micelles

copolymers	micelle supported H_2O (ppm)[a]	H_2O per IL diblock	H_2O per IL repeat unit
d,h-PS(125)−IL(7)	190	23	3.8
d,h-PS(125)−IL(18)	383	56	3.3
d,h-PS(125)−IL(33)	365	64	2.1
d,h-PS(125)−IL(46)	393	79	1.9

[a] Duplicate measurements showed the error margin for the measurement is ~ ±10 ppm.

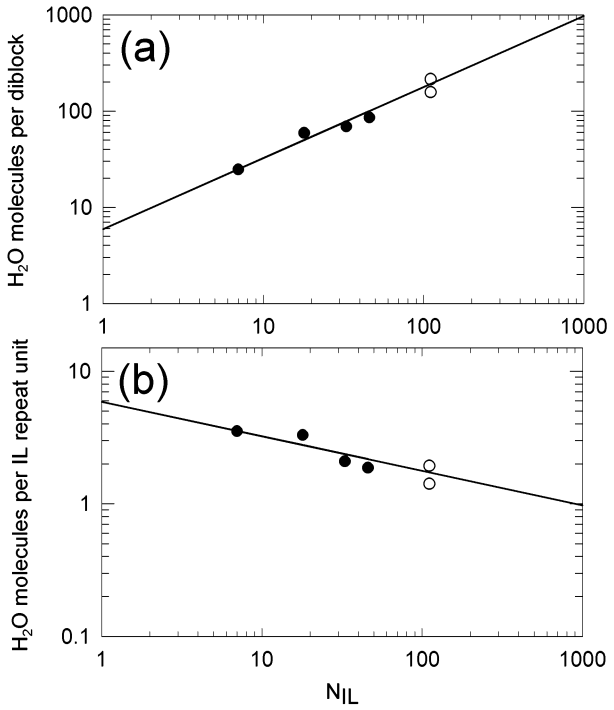

Figure 9. The results of the water content measurements of the copolymer toluene solutions saturated with water are reported as (a) the number of water molecules per each diblock and (b) the number of water molecules per each IL repeat unit as a function of the IL block length, N_{IL}. The closed circles are for the copolymers discussed in this article, while the open circles are for a similar copolymer from an earlier study.[27]

Using Karl Fischer titration, we quantify the amount of water in the micelle solutions (Table 5) and confirm that trace amounts of water are solublized by the micelle solutions. We measure 510 ppm of water for saturated toluene, which is comparable to the literature value.[60] We then take the excess water over 510 ppm found in the copolymer micelle solutions to be water supported by the micelle structures, as reported in Table 5.

While we can quantify the amount of water solublized by the micelle structures, we would like to consider how the micelle structures contain this water. As imidazolium structures with BF_4^- counterions in the bulk exposed to water have been shown to take up 20 000 and 14 000 ppm of water,[61] we believe that the water in our copolymer solutions is associating with these functionalities in the IL block of the micelle core. Our data indicate that the amount of water supported by each IL repeat unit is not

(56) Nagarajan, R. *Polym. Adv. Technol.* **2001**, *12*, 23−43.
(57) Khougaz, K.; Gao, Z. S.; Eisenberg, A. *Langmuir* **1997**, *13*, 623−631.
(58) Cogan, K. A.; Gast, A. P. *Macromolecules* **1990**, *23*, 745−753.
(59) Schmidt, M.; Paradossi, G.; Burchard, W. *Makromol. Chem., Rapid Commun.* **1985**, *6*, 767−772.
(60) Smallwood, I. M. *Handbook of Organic Solvent Properties*; Halsted Press: New York, 1996.
(61) Cammarata, L.; Kazarian, S. G.; Salter, P. A.; Welton, T. *Phys. Chem. Chem. Phys.* **2001**, *3*, 5192−5200.

constant through the copolymer series, as shown in Figure 9. The water per IL repeat unit is largest for the copolymer with the shortest IL block and steadily decreases with the IL block length. This leads us to consider that the water must not be evenly distributed throughout the micelle cores but that the IL units at the ends of the diblock chains may be able to support more water than the IL units closer to the PS interface. We previously proposed the possibility that the packing constraints of the extended IL blocks could create a central cavity in the micelle core. In this case, water may pool in the cavity rather than associating uniformly with the IL units along the length of the IL block. This is consistent with our finding that the micelle cross-sectional dimension and flexibility are not substantially altered with the addition of water.

V. Conclusions

We report on our studies of a series of *d*,*h*-PS−IL diblock copolymer micelles using contrast matching with SANS. We find that these copolymers form elongated micelles that have relatively short, semiflexible, cylindrical IL cores surrounded by a diffuse PS shell. The dimensions of the micelle cores can be linearly related to the IL block length and suggest that the IL blocks are fully extended across the micelle core. Furthermore, the relationships between the IL block length and the micelle core length and features in the scattering data indicate the cylindrical core structures are relatively monodisperse. As the length of the IL core-forming block is increased, the conformation of the PS shell changes from starlike to brushlike. With this shift to a more brushlike PS shell conformation comes an increase in the volume fraction of PS in the micelle shell. The aggregation of the copolymers into self-assembled micelles seems to be driven by the association of the IL blocks forming the micelle core. Furthermore, the micelle morphology appears to be dictated by the packing of the IL blocks. When the micelle solutions are saturated with water, the water partitions into the micelle structures. The quantity of water supported by the micelles indicates that the IL units at the ends of the copolymer chain can support more water. While saturation with water does not alter the length or flexibility of the micelles, it does slightly swell their cross-sectional dimensions. We believe that through our study of this system we have helped to elucidate the phenomena surrounding the structure and aggregation of nonspherical block copolymer micelles. We aim to further explore the details of these micelle structures and their utility in applications such as catalysis.

Acknowledgment. We thank Professor Nitash Balsara for use of his DLS instrument and Mr. Timothy J. Rappl for assistance with these experiments. We acknowledge support for this work from the NSF Center for Polymer Interfaces and Macromolecular Assemblies (CPIMA), Grant No. DMR-9808677. We acknowledge the support of the National Institute of Standards and Technology, U.S. Department of Commerce, in providing facilities used in this work. This material is based upon activities supported by the National Science Foundation under Agreement No. DMR-9986442. A.R.L. thanks the National Institutes of Health for a postdoctoral fellowship (66597-01). We thank the reviewers for their insightful comments and corrections to the manuscript.

LA0364183